Journal of Polymer Science & Applications

Research Article

Synthesis and Characterization of Electroactive Fluorinated Poly (Amic Acid) Bearing Oligoaniline Pendants

**Ying Yan, Yanyan Li and Danming Chao***

Abstract

A novel electroactive fluorinated poly (amic acid) (EFPAA) was firstly synthesized in a single step from 4,4'-(Hexafluoroisopropylidene) diphthalic anhydride (HFDA) and electroactive diamine monomer (EDA). The structure of EFPAA was confirmed by Fourier-transform infrared spectra (FTIR), nuclear magnetic resonance (NMR) and gel permeation chromatography (GPC). The electroactivity of EFPAA was evaluated by performing electrochemical cyclic voltammetry in 0.5 M H_2SO_4 confirming a surface-controlled process. EFPAA/ITO electrode displayed good electrochromic behavior with high contrast value, moderate switching times, acceptable coloration efficiency. Moreover, anticorrosion performance of the EFPAA coatings on the stainless steel (SS) in 3.5 wt % NaCl solution was investigated by tafel plot analysis and electrochemical impedance spectroscopy. A comprehensive and detailed study of corrosive protection of EFPAA will provide an insightful tool for developing electrochromic displays and anticorrosive paint.

Keywords

Polyaniline; Fluorinated, Electrochromic; Anticorrosion

Graphical Abstract
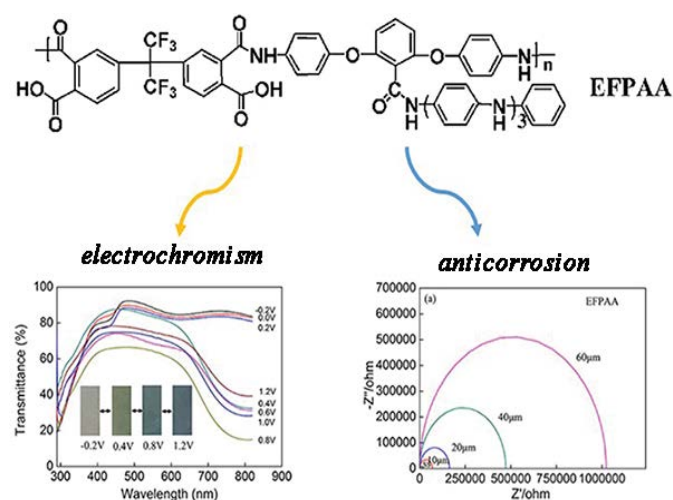
*Corresponding author: Danming Chao, College of Chemistry, Jilin University, Changchun, 130012, P.R. China, Tel: +86-431-85168292; Fax: +86-431-85168292; E-mail: chaodanming@jlu.edu.cn

We report the synthesis of a novel electroactive fluorinated poly(amic acid) (EFPAA) containing tetraaniline pendants. The expected electrochromic behavior was observed through the electrochemical measurement of EFPAA/ITO electrode. Moreover, the as-prepared EFPAA also shows outstanding anticorrosive performance for stainless steel.

Introduction

As one of the most heat-resistant polymers, polyimides are widely used in high temperature plastics, adhesives, sealants, photoresists, separation membranes, dielectrics, coatings, and optical materials [1]. Due to their good thermal, chemical and mechanical properties, polyimides are utilized as stable coatings for anticorrosion [2-4]. Recently, researchers have intensely focused on the preparation of improved anticorrosive polyimide coatings to resolve the water penetration issue. First, some inorganic materials, such as silica [5], clay [6], boron nitride [3] and graphene [7] have been imported into the polymer matrix. The resulting polyimide/inorganic composites coatings exhibit better water resistance and better anticorrosion behavior. Moreover, the fabrication of super hydrophobic nanostructured polyimide surfaces would be another effective strategy to improve corrosion protection [4,8] Improved anticorrosion should be resulted from super hydrophobicity and dual barrier protection. To expand practical applicability, more polyimide materials need to be explored, with emphasis on materials with good anticorrosive properties.

Among the conducting polymers, polyaniline (PANI) is considered to be one of the most promising materials in anticorrosive coatings as an alternative to chromium-containing systems due to its high conductivity, good environmental stability, easy synthesis and relatively low cost [9-13]. PANI coatings can provide sacrificial cathodic protection as well as a physical barrier against any aggressive corrosion. During the anticorrosive process, a metal passivation phenomenon has been observed, which could be ascribed to the redox catalytic effect of PANI [14,15]. Recently, several kinds of polyaniline-type anticorrosive materials have been designed and prepared, such as polyaniline-salts with various dopant types [16,17], polyaniline-inorganic nanocomposites with graphite, TiO_2, $ZnMoO_4$, ZnAl-LDH [18-21], polyaniline-polymers composites/blends [22-25]. However, the poor solubility and process ability of polyaniline will impede its development in anticorrosion applications. Although re-doping techniques, sulfonating methods, and other modified means could partially solve the above problem, more convenient and effective methods should be explored.

To improve the solubility and process ability, a new approach incorporating the oligoanilines into other polymeric systems, has recently emerged. With the design and synthesis of various monomers, electroactive polymers containing oligoanilines have attracted much attention both in fundamental and applied research in fields of electroluminescent devices, electrochromic materials, sensors, etc. [26-30]. As a result, electroactive polymers with different topological structures, such as graft, alternating, hyperbranched and block-like polymers [26-33], have been synthesized and reported. Herein, considering the protective nature of polyimide and the versatility of PANI-based materials, a novel precursor of polyimide with

oligoaniline segments was designed and synthesized. The structure, electroactivity and electrochromic properties of the obtained polymer were studied. Furthermore, the corrosive protection of EFPAA for SS was investigated in detail.

Experimental

Materials

4,4'-(Hexafluoroisopropylidene) diphthalic anhydride and 4,4'-(1,3-phenylenedioxy) dianiline were purchased from Sigma-Aldrich. Ammonium persulfate (APS), ferric chloride, and potassium carbonate were obtained from Tianjin Chemical Factory. Hydrochloric acid (37%) and ammonia water (25%) were purchased from Shenyang Chemical Factory. N,N'-Dimethylformamide (DMF), N,N'-dimethylacetamide (DMAc), tetrahydrofuran, toluene, dichloromethane and ethanol were obtained from commercial sources and used as received without further purification. EDA was prepared in our lab by an established synthetic route [30]. Optically transparent indium-tin oxide (ITO) glass substrates were obtained from Reintech electronic technologies Co. Ltd (Beijing) and used as working electrode substrates in the electrochemical measurements. The composition of stainless steel (SS, T301), used in the anticorrosion tests is as following (wt %): C 0.15%, Si 1.0%, Mn 2.0%, Cr 16.0~18.0%, Ni 6.0~8.0%, S 0.03%, P 0.045% and Fe bal.

Structure characterization of EFPAA

Mass spectra were performed on an AXIMA-CFR laser desorption ionization time of flight mass spectrometer (COMPACT). Fourier transform infrared (FTIR) spectra were recorded on a BRUKER VECTOR 22 Spectrometer by averaging 128 scans at a solution of 4 cm^{-1} in the range of 4000-400 cm^{-1}. NMR spectra in deuterated dimethyl sulfoxide (DMSO) were acquired using a Bruker-500 spectrometer at room temperature.

Molecular weight of EFPAA

The molecular weight information of EFPAA was collected using Shimadzu gel permeation chromatography (GPC) unit equipped with a Shimadzu GPC-802D gel column and SPD-M10AVP detector. N,N'-Dimethylformamide (DMF) was used as the eluent at a flow rate of 1 mL/min. Before analysis, the sample was filtered through a 0.2 mm poly (tetrafluoroethylene) syringe filter. Calibration was accomplished with monodispersed polystyrene standards with a molecular weight range from 500 to 500000 g/mol.

Thermal analysis of EFPAA

The thermal stability of EFPAA was studied on Perkin-Elmer PYRIS 1 TGA in the temperature range of 100-680°C at a rate of 10°C/min under nitrogen atmosphere. Before testing, the EFPAA was kept under nitrogen atmosphere at 120ºC for 0.5 h to remove any residual water and/or solvents.

Electrochemical properties of EFPAA

The electrochemical properties of EFPAA, including electroactivity, electrochromic performance, polarization curve and electrochemical impedance spectroscopy, were investigated on a CHI 660A Electrochemical Workstation (CH Instruments, USA) with a conventional three electrode cell, using a saturated calomel electrode (SCE) as the reference electrode, a platinum wire electrode as the counter electrode, and the EFPAA-decorated working

electrode. Moreover, the spectroscopic properties of EFPAA in the electrochromic measurements were studied using a UV-3101 PC spectrometer (SHIMADZU).

Anticorrosive performance of EFPAA

The anticorrosive performance of EFPAA and the referential polymer for the SS in 3.5 wt % NaCl corrosive solution was studied by polarization curve technique and electrochemical impedance spectroscopy. EFPAA/SS electrode was applied as the working electrode in the traditional three electrode system.

In the polarization curve measurements, the electrochemical corrosion parameters were calculated using the following equations. First, the polarization resistances (R_p) were calculated from the Tafel curves according to the Stearn-Geary equation [34-36]:

$$Rp = \frac{b_a b_c}{2.303 \left(b_a + b_c \right) I_{corr}}$$

where I_{corr} is corrosion current (A/cm^2), b_a and b_c are the anodic and cathodic Tafel slope ($\Delta E/\Delta log\ I$), respectively. Corrosion rate (R_{corr}, in mm per year) was evaluated using the following equation [37,38]:

$$R_{corr} = \frac{I_{corr} M}{DV} \times 3270$$

Where I_{corr} is the corrosion current density (A/cm^2), M is the molecular weight of the metal subjected to corrosion (g/mol), V is the valence, 3270 is the constant and D is the density of the corroding metal (g/cm^3). The protection efficiency ($P_{EF\%}$) values were estimated using the equation [39,40]:

$$P_{EF}\% = \frac{R_p^{-1} \left(uncoated \right) - R_p^{-1} \left(coated \right)}{R_p^{-1} \left(uncoated \right)} \times 100$$

Where R_p(uncoated) is the polarization resistances of bare SS substrate, R_p(coated) is the polarization resistances of SS substrate coated with polymers.

Synthesis of EFPAA and NPAA

EFPAA was synthesized in a single step as depicted in Figure 1. Firstly, 2.053 g EDA and 1.333 g HFDA were dissolved in 15 mL DMAc in a three-necked round-bottom flask. The mixed solution was stirred for 24 h under nitrogen atmosphere at room temperature. The resultant 20 wt % EFPAA DMAc solution was placed in the freezer.

EFPAA (KBr, cm^{-1}): 3411(v_{N-H}), 2969(v_{C-H}), 1659($v_{C=O}$), 1570($_{C=C}$ of benzenoid rings), 1501($v_{C=C}$ of benzenoid rings), 1316(v_{C-N}), 1255(v_{C-O-C}), 1100-1250(v_{C-F}), 852(δ_{C-H}), 748(δ_{C-H}), 685(δ_{C-H}). ^{1}H-NMR (d$_6$-DMSO): δ=13.60 (m, -COOH), δ=10.60 (s, Ar-NH-CO-), δ=10.4(s, Ar-NH-CO-), δ=8.90(m, N-H), δ=7.29-6.84(m, Ar-H). GPC results: Mn: 55960, Mw: 108250, PDI: 1.93.

Furthermore, a referential polymer was prepared through the same synthetic strategy using 4,4'-(1,3-phenylenedioxy)dianiline as the diamine monomer so as to clarify the effect of oligoaniline segments on the anticorrosion property. The resulting poly(amic acid) was named NPAA and also depicted in Figure 1.

NPPA (KBr, cm^{-1}): 3419(v_{N-H}), 3000(v_{C-H}), 1598($v_{C=C}$ of benzenoid rings), 1504($v_{C=C}$ of benzenoid rings), 1417(v_{C-N}), 1265(v_{C-O-C}), 1100-1260(v_{C-F}), 846(δ_{C-H}), 733(δ_{C-H}), 683(δ_{C-H}). ^{1}H-NMR (d$_6$-DMSO): δ=13.58 (m, -COOH), δ=10.70(m, Ar-NH-CO-), δ=8.07 (m, N-H), δ=7.91-6.98(m, Ar-H). GPC results: Mn: 65460, MW: 114670, PDI: 1.75.
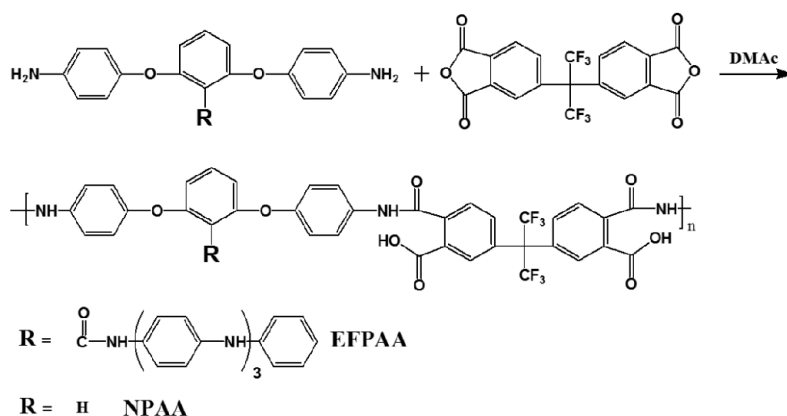
Figure 1: Synthetic route of EFPAA and the structure of NPAA.

Fabrication of EFPAA/ITO electrodes and NPAA/SS electrodes

ITO substrates were washed ultrasonically with acetone and distilled water for 3 min each, followed by drying in the air. EFPAA DMAc solution was filtered through 0.2 μm syringe filter, and then spin-coated onto the ITO substrate for spectroelectrochemical measurements. The spin-coating process started at 500 rpm for 9 s and then 1000 rpm for 30 s. The EFPAA films, with thickness of 300 nm, were used in the electroactivity and electrochromism measurement.

For the anticorrosion measurements, the SS substrates were prepared with $1.0 \times 1.0 \times 0.1$ cm dimension and polished with emery papers. Then they were washed and degreased ultrasonically with acetone, distilled water and acetone again, followed by drying in a vacuum oven. The filtered polymer DMAc solution was cast onto treated SS substrates and then dried in the air to give the electrodes. The thickness of anticorrosive coatings was controlled by adjusting the concentration of polymer solution and/or increasing the times of dripping.

Results and Discussion

EFPAA structure

EFPAA was synthesized using a one-step synthetic route as depicted in Figure 1. EFPAA, ^{1}H NMR spectroscopy and GPC were applied to confirm the chemical structure of as-synthesized EFPAA. EFPAA spectrum displays the characteristic absorption bonds around 3411 cm^{-1} corresponding to the N-H stretching vibration, around 2969 cm^{-1} due to the C-H stretching vibration of aryl groups. The vibration around 1659 cm^{-1} is attributed to C=O stretching vibration. The chracteristic peaks at 1570 cm^{-1} and 1501 cm^{-1} were designated as the streching vibration of C=C groups in the benzene rings. Moreover, the bands at 1316 cm^{-1} (υ_{C-N}), 1255 cm^{-1} (υ_{C-O-C}), 1100-1250(υ_{C-F}), 852(δ_{C-H}), 748(δ_{C-H}), 683(δ_{C-H}), based on the structure of EFPAA are also observed. In the ^{1}H NMR spectra of EFPAA, the characteristic proton signal of carboxylic acids appears at 13.6 ppm. The proton signals observed at 10.6 ppm and 10.4 ppm are attributed to the protons of amide groups. The signals in the range of δ=7.29-6.84 ppm are ascribed to the aromatic protons. All of the information from FTIR spectrum and ^{1}H NMR spectrum support the expected molecular structure of EFPAA. Moreover, the number average molecular weight (Mn) and polydispersity index of EFPAA, obtained by GPC, are 55960 and 1.93.

Thermal properties

The thermal properties of EFPAA were evaluated by TGA. As shown in Figure 2, a clear three-step decomposition path is observed for the obtained EFPAA. The first weight loss began at 170°C with a mass loss of 8 %, which was attributed to the progress of imidization and the evaporation of residual solvents. The second weight loss occurred in the temperature range of 330-430°C with a mass loss of 3% which corresponds to the achievement of imidization. The following weight loss after 500°C was assigned to the decomposition of the polymer main chain. When the temperature increases to 600°C, the weight loss is about 27%. When the temperature increases to 680°C, approximately 63% of the material remains. These results indicated that the imidized EFPAA exhibits good thermal stability and high degradation temperature, compared with other PANI materials [41].

Electrochemical activity

Cyclic voltammetry (CV) was performed to explore the electrochemical activity of EFPAA. In the traditional three-electrode system, the platinum wire electrode, saturated calomel electrode and EFPAA/ITO electrode were used as counter electrode, reference electrode and working electrode, respectively. The liquid electrolyte was 0.5 M H_2SO_4 solution. The CV curve of EFPAA/ITO is shown in Figure 3 and reveals two pairs of redox peaks at 310 mV/180 mV and 465 mV/385 mV. The first pair of redox peaks at 310 mV/180 mV should be attributed to the transition between the leucoemeraldine base (LEB) and the emeraldine base (EB), and the second pair of redox peaks should be assigned to the transition between EB and the pernigraniline base (PNB). Furthermore, CV of EFPAA was also carried out with the potential scan rate in the range of 10~100 mV/s. A linear dependence of the peak currents, as a function of scan rates, is seen in the inset of Figure 3, which confirmed a surface controlled process.

Electrochromic behavior

Polyaniline (PANI) is considered to be one of the most promising electrochromic materials due to its high optical contrast, good redox reversibility and electrochemical stability. Due to the introduction of oligoaniline, the synthesized EFPAA should be investigated as an electrochromic polymer. Firstly, the optical properties of EFPAA during the oxidation process were investigated by UV-vis spectroscopy Figure 4. When the oligoaniline segment is in its reduced state, only one strong absorption around 325 nm is observed in the
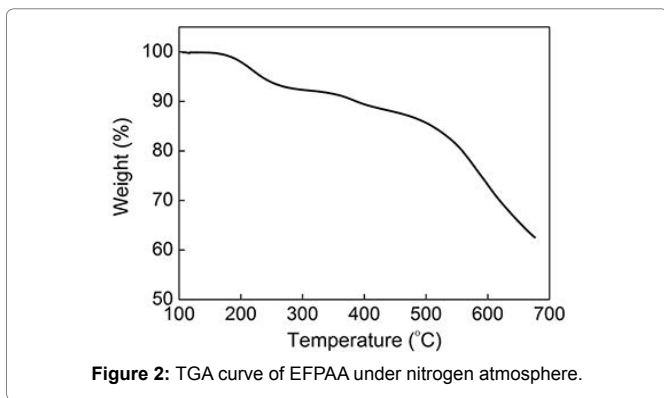
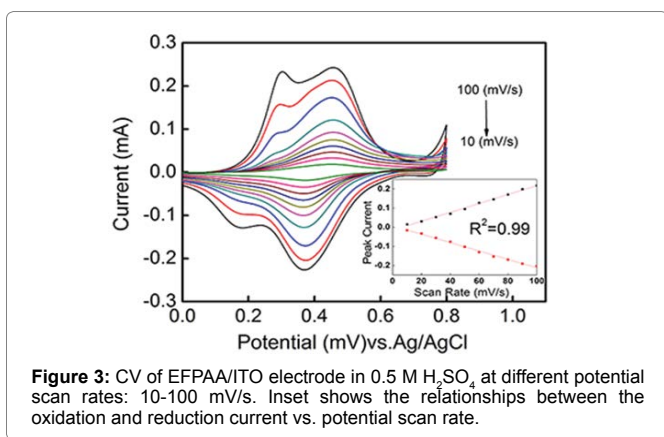**Figure 2:** TGA curve of EFPAA under nitrogen atmosphere.

Figure 3: CV of EFPAA/ITO electrode in 0.5 M H_2SO_4 at different potential scan rates: 10-100 mV/s. Inset shows the relationships between the oxidation and reduction current vs. potential scan rate.

UV-vis spectra, which should be associated with a π–π* transition of the conjugated ring system [42,43]. After the addition of ammonium persulfate, the absorption band of the π–π* transition continually decreased in intensity and underwent a blue shift. Meanwhile, a new absorption band appeared at 570 nm and continually increased in intensity, which is assigned to exciton-type transition between the HOMO orbital of the benzoid ring and the LUMO orbital of the quinoid ring in oligoaniline segment [42,43]. When the oligoaniline segment was oxidized to EB, the intensity of π-polaron transiting absorption reached a maximum. After that, the absorption peak of exciton-type transition decreased gradually with further oxidation.

The above spectroscopic properties of EFPAA are consistent with those of polyaniline, which indicate that the EFPAA shows great potential as an electrochromic material. Therefore, the electrochromic behavior of EFPAA was investigated in detail by spectroelectrochemical experiments, which were performed in 0.5 mol/L H_2SO_4 coupled with applied potentials (-0.2 V, 0.2 V, 0.4 V, 0.6 V, 0.8 V, 1.0 V and 1.2 V (vs. Ag/AgCl)). As shown in Figure 5, the EFPAA film shows different UV-Vis absorption spectra at various applied potentials, exhibiting the maximum optical contrast value (%ΔT) about 55% at 700 nm between its coloring (0.8 V) and bleaching (-0.2 V) states. Moreover, the color of EFPAA film changes drastically from transmissive gray (-0.2 V), to green (0.4 V), and finally to absorptive black blue (at 0.8 V) (inset of Figure 5).

Furthermore, the switching time and the electrochromic efficiency were also studied in detail by spectrochronoamperometry, which was conducted in the optical contrast at 700 nm during repeated potential stepping between reductive (-0.2 V) and oxidative state at 0.8 V with a residence time of 30 s. The results for the first 500 s were presented in

the Figures 6a and 6b. From the electrochemical curves, the switching time of EFPAA film is about 5.2 s at 0.8 V for the coloring process at 700 nm. The EFPAA film requires 4.0 s at -0.2 V for the bleaching process, which is moderate for a polymeric electrochromic material. In addition, the electrochromic coloration efficiency (CE) is calculated for 45.4 cm²/C (at 700 nm) at the oxidation stage by monitoring the amount of ejected charge (Q) as a function of the change in optical density (ΔOD) of the EFPAA film.

Anticorrosion performance

Considering the good electrochemical activity of EFPAA, the anticorrosive performance is investigated here in detail. To clarify the effect of oligoaniline segments on the anticorrosion properties, a referential polymer without electroactive segment (NPAA) was also studies. Firstly, the polarization technique was used to study the anticorrosion performance of EFPAA and NPAA for SS, where the large cathodic and anodic polarizations provide curves for the respective corrosion processes. The corrosive solution is 3.5 wt % NaCl solutions. The anticorrosive coatings were cast with thickness of 10 μm, 20 μm, 40 μm and 60 μm by dripping method. From the Tafel curves (Figure 7), both corrosion potential (E_{corr}) and corrosion current density (I_{corr}) of all the samples are determined according to Tafel extrapolation method, and listed in Table 1. In case of the bare SS sample, the E_{corr} and I_{corr} are -0.744 V and 6.277 μA/cm², respectively. When NPAA is used as the anticorrosive coating with the thickness of 10 μm, 20 μm, 40 μm and 60 μm, the E_{corr} shifts to 0.300 V, 0.453 V, 0.912 V, 1.446 V and the I_{corr} decreases drastically to 1.178 μA/cm², 0.637 μA/cm², 0.039 μA/cm², 0.027 μA/cm². All the above results demonstrate the corrosion protection of the NPAA coatings. After coated by EFPAA with thickness of 10 μm, 20 μm, 40 μm and 60 μm, the E_{corr} shift significantly positively to 0.399 V, 0.584 V, 1.381 V and 2.169 V, which confirm an effective corrosive protection, is provided by the EFPAA coatings. The I_{corr} is also found
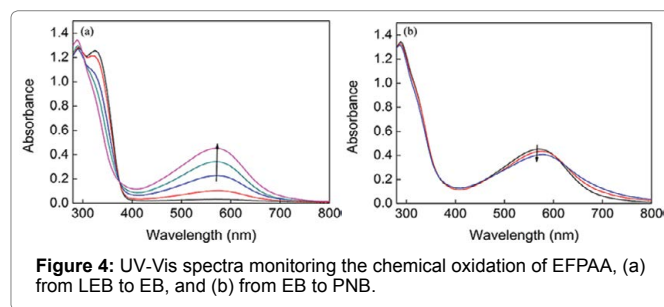

Figure 4: UV-Vis spectra monitoring the chemical oxidation of EFPAA, (a) from LEB to EB, and (b) from EB to PNB.
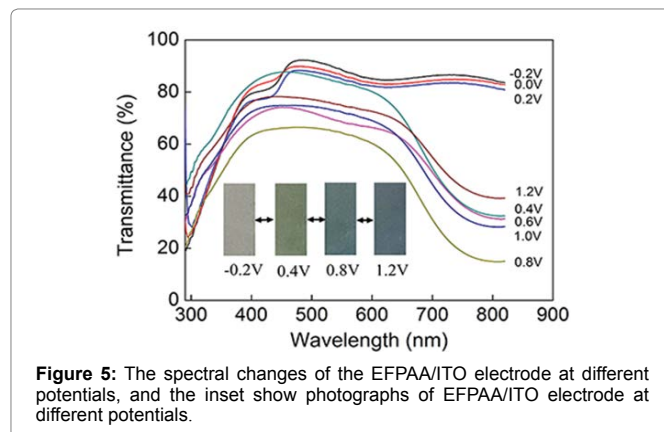

Figure 5: The spectral changes of the EFPAA/ITO electrode at different potentials, and the inset show photographs of EFPAA/ITO electrode at different potentials.
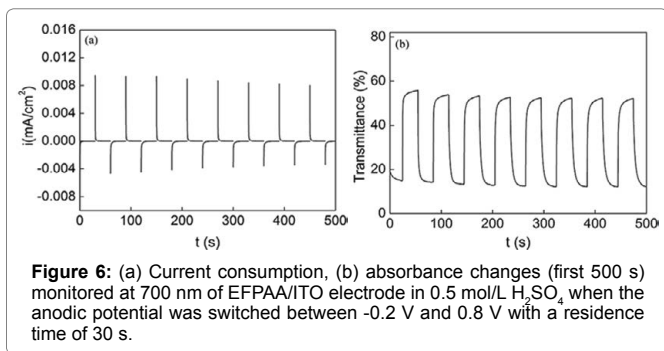
Figure 6: (a) Current consumption, (b) absorbance changes (first 500 s) monitored at 700 nm of EFPAA/ITO electrode in 0.5 mol/L H_2SO_4 when the anodic potential was switched between -0.2 V and 0.8 V with a residence time of 30 s.
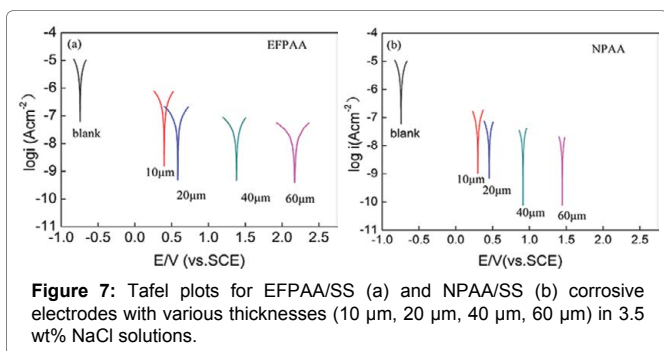

Figure 7: Tafel plots for EFPAA/SS (a) and NPAA/SS (b) corrosive electrodes with various thicknesses (10 µm, 20 µm, 40 µm, 60 µm) in 3.5 wt% NaCl solutions.

Table 1: Electrochemical corrosion parameters of the EFPAA/SS and NPAA/SS samples with various thicknesses (10 µm, 20 µm, 40 µm, 60 µm) in 3.5 wt% NaCl solution.

| Sample	Ecor (V)	Icorr (µ/cm²)	Rp (kΩ/cm²)	Rcorr (mm/year)	P_{EF} (%)
SS	-0.774	6.277	0.149	4.83×10^{-2}	..
NPPA-10 µm	0.3	1.178	0.887	9.06×10^{-2}	83.19
NPPA-20 µm	0.453	0.637	1.55	4.90×10^{-3}	90.38
NPPA-40 µm	0.912	0.039	5.181	2.94×10^{-4}	97.12
NPPA-60 µm	1.446	0.027	8.934	2.07×10^{-4}	98.33
EFPPA-10 µm	0.339	0.259	4.096	2.90×10^{-3}	96.36
EFPPA-20 µm	0.584	0.043	25.592	3.31×10^{-4}	99.41
EFPPA-40 µm	1.381	0.029	36.67	2.21×10^{-4}	99.59
EFPPA-60 µm	2.169	0.011	85.335	8.54×10^{-5}	99.83
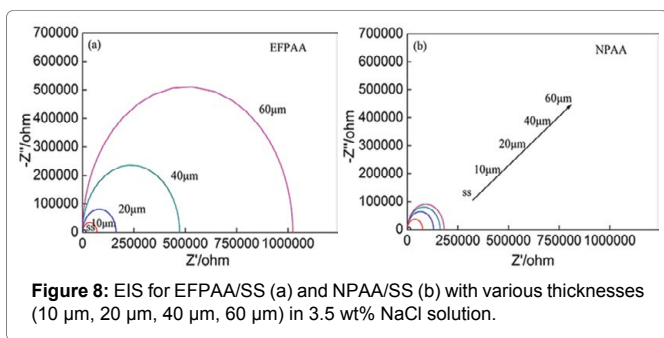
Figure 8: EIS for EFPAA/SS (a) and NPAA/SS (b) with various thicknesses (10 µm, 20 µm, 40 µm, 60 µm) in 3.5 wt% NaCl solution.

to decrease drastically to 0.259 µA/cm², 0.043 µA/cm², 0.029 µA/cm² and 0.011 µA/cm² indicating that the overall corrosion process is also reduced significantly.

According to the related equations, other electrochemical corrosion parameters of the samples, such as R_p value, R_{corr} and P_{EF}, were calculated and presented in Table 1. The R_p value of EFPAA/SS samples increase from 0.149 to 85.335 kΩ cm² as the thickness

of EFPAA increase from 0 to 60 µm in 3.5 wt % NaCl solution. In contrast, the R_p value of NPAA/SS increases to 8.934 kΩ cm² when the thickness increases to 60 µm. As shown in Table 1, R_{corr} is found to be 4.83×10^{-2} mm per year for the bare SS. The R_{corr} of EFPAA coating with thickness of 60 µm decreases greatly to 8.54×10^{-5} mm per year, giving a high P_{EF} (99.83%). In contrast, the R_{corr} of NPAA is about 2.07×10^{-4} mm per year, which is bigger than that of EFPAA. Through the comparative and detailed study of the anticorrosive coatings, the effect of the oligoaniline segment on the anticorrosion has been illuminated, which can be attributed mainly to the presence of π-electron clouds coexisting with nitrogen atom [44,45].

Electrochemical impedance spectroscopy (EIS) was also used to investigate the anticorrosion behavior of EFPAA and NPAA coatings. All the Nyquist plots of the samples, fitted by equivalent circuit, are presented in Figure 8, which are close to a semicircle arc. The Randles type equivalent circuit model was chosen to simulate the experimental data at the initial state. The film resistance (R_f) for the samples is determined by the intersection of the low-frequency end of the semicircle arc with the real axis. For the bare SS samples, the R_f of the bare SS is 17742 Ω. The R_f of NPAA/SS samples increases to 69640 Ω, 162710 Ω, 472052 Ω and 1022856 Ω as the thickness of EFPAA film increased to 10 µm, 20 µm, 40 µm and 60 µm. For the EFPAA/SS samples, the R_f values are 75710 Ω, 12984 Ω, 161966 Ω and 181951 Ω as the thickness increased to 10 µm, 20 µm, 40 µm and 60 µm. Comparing all the R_f values of the samples, the higher R_f values of EFPAA would demonstrate the availability of the oligoaniline segments to prevent the corrosion of SS, which also implies that the prepared EFPAA coating offers excellent corrosion protection to SS in the brine.

Conclusion

EFPAA, with pendant tetraaniline and fluorine groups, was synthesized by simple polycondensation chemistry. The novel polymer exhibits good thermal stability and reversible electrochemical properties. EFPAA film reveals good electrochromic performance with high contrast value, moderate switching times and acceptable coloration efficiency. The effective anticorrosion behaviors of the EFPAA coatings were confirmed by tafel plots analysis and electrochemical impedance spectroscopy, which indicated the promise as competitive anticorrosion materials. The detailed investigation of EFPAA not only paves the way for its practical application, but has also inspired us to explore new characteristics for polymer materials with various functional groups.

References

1. Liaw D, Wang K, Huang Y, Lee K, Lai J, et al. (2012) Advanced polyimide materials: Syntheses, physical properties and applications. Prog Polym Sci 37: 907-974.

2. Huttunen-Saarivirta E, Yudin V, Myagkova L, Svetlichnyi V (2011) Corrosion protection of galvanized steel by polyimide coatings: EIS and SEM investigations. Prog Org Coat 72: 269-278.

3. Huang Y, Lo T, Chao C, Whang W (2014) Anti-corrosion characteristics of polyimide/h-boron nitride composite films with different polymer configurations. Surf Coat Tech 260: 113-117.

4. Lo T, Huang Y, Hsiao Y, Chao C, Whang W (2014) Preparation of super hydrophobic polyimide films modified with organosilicasol as effective anticorrosion coatings. Surf Coat Tech 258: 310-319.

5. Hung W, Weng C, Lin Y, Chung P, Tsai S, et al. (2010) Enhanced anticorrosion coatings prepared from Incorporation of well-dispersed silica nanoparticles into fluorinated polyimide matrix. Polym Composite 31: 2025-2034.

6. Chang K, Huang H, Lai M, Hung C, Chand B, et al. (2009) Comparative electrochemical studies at different operational temperatures for the effect of nanoclay platelets on the anticorrosion efficiency of organo-soluble polyimide/clay nanocomposite coatings. J Nonsocial Nanotechnol 9: 3125-3133.

7. Chang K, Hsu C, Lu H, Ji W, Chang C, et al. (2014) Advanced anticorrosive coatings prepared from electroactive polyimide/graphene nanocomposites with synergistic effects of redox catalytic capability and gas barrier properties. Express Polym Lett 8: 243-255.

8. Chang K, Lu H, Peng C, Lai M, Hsu S, et al. (2013) Nanocasting technique to prepare lotus-leaf-like super hydrophobic electroactive polyimide as advanced anticorrosive coatings. ACS Appl Mater Interfaces 5: 1460-1467.

9. Anderson M, Mattes B, Reiss H, Kaner R (1991) Conjugated polymer films for gas separations. Science 252: 1412-1415.

10. Zhang H, Wang X, Li J, Mo Z, Wang F (2009) Conducting polyaniline film from aqueous dispersion: crystallizable side chain forced lamellar structure for high conductivity. Polymer 50: 2674-2679.

11. Chen Y, Wang X, Li J, Lu J, Wang F (2007) Polyaniline for corrosion prevention of mild steel coupled with copper. Electrochim Acta 52: 5392-5399.

12. Li Y, Zhang H, Wang X, Li J, Wang F (2011) Growth kinetics of oxide films at the polyaniline/mild steel interface. Corros Sci 53: 4044-4049.

13. Yang T, Peng C, Lin Y, Weng C, Edgington G, et al. (2012) Synergistic effect of electroactivity and hydrophobicity on the anticorrosion property of room-temperature-cured epoxy coatings with multi-scale structures mimicking the surface of Xanthosoma sagittifolium leaf. J Mater Chem 22: 15845-15852.

14. Chen X, Luo C, Zhang Z, Zhao M (2012) Preparation and anticorrosion properties of polyaniline-containing coating on Mg-Li alloy. Anti-Corros Method M 59: 291-298.

15. Wessling B (1998) Dispersion as the link between basic research and commercial applications of conductive polymers (polyaniline). Synth Met 93: 143-154.

16. Kohl M, Kalendova A (2015) Effect of polyaniline salts on the mechanical and corrosion properties of organic protective coatings. Prog Org Coat 86: 96-107.

17. Grgur B, Elkais A, Gvozdenovic M, Drmanic S, Trisovic T (2015) Corrosion of mild steel with composite polyaniline coatings using different formulations. Prog Org Coat 79: 17-24.

18. Akbarinezhad E (2014) Synthesis of conductive polyaniline-graphite nanocomposite in supercritical CO_2 and its application in zinc-rich epoxy primer. J Supercrit Fluid 94: 8-16.

19. Abaci S, Nessark B (2015) Characterization and corrosion protection properties of composite material (PANI+TiO2) coatings on A304 stainless steel. J Coat Technol Res 12: 107-120.

20. Bhanvase B, Darda N, Veerkar N, Shende A, Satpute S, et al. (2015) Ultrasound assisted synthesis of PANI/ZnMoO4 nanocomposite for simultaneous improvement in anticorrosion, physico-chemical properties and its application in gas sensing. Ultrasonics Sonochemistry 24: 87-97.

21. Hu J, Gan M, Ma L, Zhang J, Xie S, et al. (2015) Preparation and enhanced properties of polyaniline/grafted intercalated ZnAl-LDH nanocomposites. Appl Surf Sci 328: 325-334.

22. Adhikari A, Claesson P, Pan J, Leygraf C, Dedinaite A, et al. (2008) Electrochemical behavior and anticorrosion properties of modified polyaniline dispersed in polyvinylacetate coating on carbon steel. Electrochim Acta 53: 4239-4247.

23. Weng C, Chang C, Lin I, Yeh J, Wei Y, et al. (2012) Advanced anticorrosion coating materials prepared from fluoro-polyaniline-silica composites with synergistic effect of superhydrophobicity and redox catalytic capability. Surf Coat Tech 207: 42-49.

24. Weng C, Chen Y, Jhuo Y, Lin Y, Yeh J (2013) Advanced antistatic/anticorrosion coatings prepared from polystyrene composites incorporating dodecylbenzenesulfonic acid-doped SiO_2@polyaniline core shell microspheres. Polym Int 62: 774-782.

25. Mostafaei A, Nasirpouri F (2014) Epoxy/polyaniline-ZnO nanorods hybrid nanocomposite coatings: Synthesis, characterization and corrosion protection performance of conducting paints. Prog Org Coat 77: 146-159.

26. Huang H, Lee Y, Yeh L, Jian J, Huang T, et al. (2013) Photoactively electroactive polyamide with azo group in the main chain via oxidative coupling polymerization. Polym Chem 4: 343-350.

27. Wang S, Chao D, Berda E, Jia X, Yang R, et al. (2013) Fabrication of electroactive oligoaniline functionalized poly(amic acid) nanofibers for application as an ammonia sensor. RSC Adv 3: 4059-4065.

28. Gao J, Liu D, Sansinena J, Wang H (2004) Synthesis and characterization of electrochromic polyamides with well-defined molecular structures and redox properties. Adv Fnuct Mater 14: 537-543.

29. Wang S, Berda E, Lu X, Li X, Wang C, et al. (2013) Tuning the fluorescent response of a novel electroactive polymer with multiple stimuli. Macromol Rapid Comm 34: 1648-1653.

30. Jia X, Chao D, Liu H, He L, Zheng T, et al. (2011) Synthesis and properties of novel electroactive poly(amic acid) and polyimide copolymers bearing pendant oligoaniline groups. Polym Chem 2: 1300-1306.

31. Chao D, Lu X, Chen J, Liu X, Zhang W, et al. (2006) Synthesis and characterization of electroactive polyamide with amine-capped aniline pentamer and ferrocene in the main chain by oxidative coupling polymerization. Polymer 47: 2643-2648.

32. Wang H, Guo P, Han Y (2006) Synthesis and surface morphology of tetraaniline-block-poly(L-lactate) diblock oligorners. Macromol Rapid Commun 27: 63-68.

33. Li F, Zhou M, Wang J, Liu X, Wang C, et al. (2015) Synthesis and electrochemical properties of electroactive hyperbranched poly(aryl ether ketone) bearing oligoaniline segments. Synthetic Met 205: 42-47.

34. Stern M, Geary A (1957) Electrochemical polarization I: A theoretical analysis of the shape of polarization curves. J Electrochem Soc 104: 56-63.

35. Gamboa S, Gonzalez-Rodriguez J, Valenzuela E, Campillo B, Sebastian P, et al. (2006) Evaluation of the corrosion resistance of Ni-Co-B coatings in simulated PEMFC environment. Electrochim Acta 5: 4045-4051.

36. Duran B, Turhan M, Bereket G, Sarac A (2009) Electropolymerization, characterization and corrosion performance of poly(N-ethylaniline) on copper. Electrochim Acta 55: 104-112.

37. Weng C, Huang J, Huang K, Jhuo Y, Tsai M, et al. (2010) Advanced anticorrosive coatings prepared from electroactive polyimide-TiO_2 hybrid nanocomposite materials. Electrochim Acta 55: 8430-8438.

38. Yeh J, Huang H, Chen C, Su W, Yu Y (2006) Siloxane-modified epoxy resin-clay nanocomposite coatings with advanced anticorrosive properties prepared by a solution dispersion approach. Surf Coat Tech 200: 2753-2763.

39. Bockris J, Reddy A (1976) Modern electrochemistry. (1st edtn), John Wiley and Sons, New York, USA.

40. Jeevananda T, Siddaramaiah S, Seetharamu S, Saravanan L, Souza D' (2004) Synthesis and characterization of poly(aniline-co-acrylonitrile) using organic benzoyl peroxide by inverted emulsion method. Synthetic Met 140: 247-260.

41. Ohmura S, Moriuchi T, Hirao T (2010) Chirality organization of aniline oligomers through hydrogen bonds of amino acid moieties. J Org Chem 75: 7909-7912.

42. Shacklette L, Wolf J, Gould S, Baughman R (1988) Structure and properties of polyaniline as modeled by single-crystal oligomers. J Chem Phys 88: 3955-3961.

43. Wei Y, Wang J, Jia X, Yeh J, Spellane P (1995) Polyaniline as Corrosion Protection Coatings on Cold Rolled Steel. Polymer 36: 4535-4537.

44. Jeyaprabha C, Sahiyanarayanan S, Venkatachari G (2006) Effect of cerium ions on corrosion inhibition of PANI for iron in 0.5 M H_2SO_4. Appl Surf Sci 253: 432-438.

45. Khaled K, Hackerman N (2003) Investigation of the inhibitive effect of ortho-substituted anilines on corrosion of iron in 0.5 M H_2SO_4 solutions. Mater Chem Phys 82: 949-960.

Author Affiliation

College of Chemistry, Jilin University, Changchun, 130012, P.R. China